

Spin-resolved electronic structure of ferroelectric α -GeTe and multiferroic $\text{Ge}_{1-x}\text{Mn}_x\text{Te}$

J. Krempaský¹, M. Fanciulli^{1,2}, N. Pilet¹, J. Minár³, W. Khan³, M. Muntwiler¹, F. Bertran⁴,
S. Muff^{1,2}, A.P. Weber^{1,2}, V.N. Strocov¹, V.V. Volobuev^{5,6}, G. Springholz⁶, J. H. Dil^{1,2}

¹Swiss Light Source, Paul Scherrer Institut,
CH-5232 Villigen PSI, Switzerland

²Institute of Physics, École Polytechnique Fédérale de Lausanne,
CH-1015 Lausanne, Switzerland

³New Technologies-Research Center University of West Bohemia,
Plzeň, Czech Republic

⁴SOLEIL Synchrotron, L'Orme des Merisiers,
F-91192 Gif-sur-Yvette, France

⁵National Technical University, Kharkiv Polytechnic Institute,
Frunze Str. 21, 61002 Kharkiv, Ukraine

⁶Institut für Halbleiter-und Festkörperphysik,
Johannes Kepler Universität, A-4040 Linz, Austria

Germanium telluride features special spin-electric effects originating from spin-orbit coupling and symmetry breaking by the ferroelectric lattice polarization, which opens up many perspectives for electrically tunable and switchable spin electronic devices. By Mn doping of the α -GeTe host lattice, the system becomes a multiferroic semiconductor possessing magnetoelectric properties in which the electric polarization, magnetization and spin texture are coupled to each other. Employing spin- and angle-resolved photoemission spectroscopy in bulk- and surface-sensitive energy ranges and by varying dipole transition matrix elements, we disentangle the bulk, surface and surface-resonance states of the electronic structure and determine the spin textures for selected parameters. From our results we derive a comprehensive model of the α -GeTe surface electronic structure which fits to experimental data and first principle theoretical predictions and we discuss the unconventional evolution of the Rashba-type spin splitting upon manipulation by external B- and E-fields.

INTRODUCTION

Rashba-type effects have been first observed in quantum confined two-dimensional electronic states of semiconductor heterostructures due to the artificial structural asymmetry created at the heterointerfaces[1, 2]. The Rashba splitting of these electronic states can be tuned electrically but the splitting is rather small, limiting practical device applications. In ferroelectrics the large natural structural asymmetry due to the ferroelectric (FE) lattice displacements leads to a large Rashba splitting even of the bulk bands for which reason such materials have been named ferroelectric Rashba semiconductor (FERS)[3]. The most prominent example is α -GeTe featuring a record spin splitting and Rashba parameters [4]. From the technological point of view GeTe also belongs to a class of chalcogenide phase-change materials [5, 6] and it is the ferroelectric semiconductor with the simplest conceivable binary structure [7, 8] with strongly asymmetric arrangement of the Ge and Te atoms along the $\langle 111 \rangle$ direction [4].

Recently, α -GeTe has attracted a flurry of experimental activity [4, 9–13] because of its giant Rashba effect, theoretically predicted by S. Picozzi [3, 14]. The highly non-centrosymmetric arrangement of the Ge and Te atoms along the $\langle 111 \rangle$ direction combined with the large spin-orbit coupling is at the heart of this effect, resulting in the highest reported bulk Rashba coupling parameter α_R of 4.25 eV \AA [4]. Doping of GeTe with Mn leads to additional ferromagnetic (FM) coupling leading to multiferroicity in $\text{Ge}_{1-x}\text{Mn}_x\text{Te}$ already for moderate Mn doping [10]. Ferroelectricity

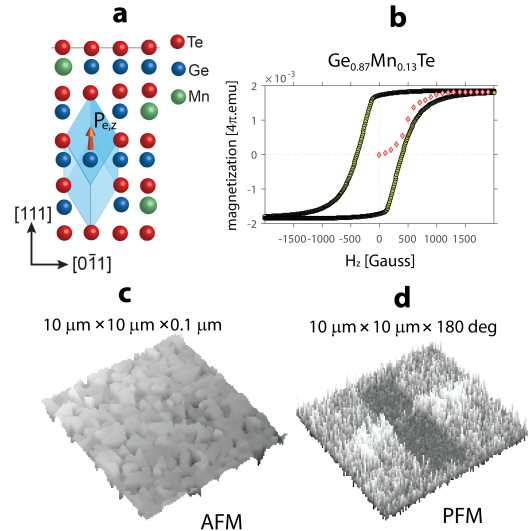


FIG. 1. (a) Sketch of multiferroic $\text{Ge}_{1-x}\text{Mn}_x\text{Te}$ with ferroelectric displacement of Ge(Mn)-atoms inside the rhombohedrally distorted unit cell along $[111]$ as indicated by the orange arrow. (b) Out-of-plane ferromagnetic hysteresis curve of multiferroic $\text{Ge}_{0.87}\text{Mn}_{0.13}\text{Te}$ measured by SQUID. (c) Surface topography measured in atomic force microscopy (AFM). (d) Piezo-force microscopy (PFM) showing 180° phase change in writing domains forming a cross. The experimental setup is measuring AFM and PFM data simultaneously.

is induced by the lattice distortion of GeTe and ferromagnetism by the coupling of the local spins of the Mn ions via

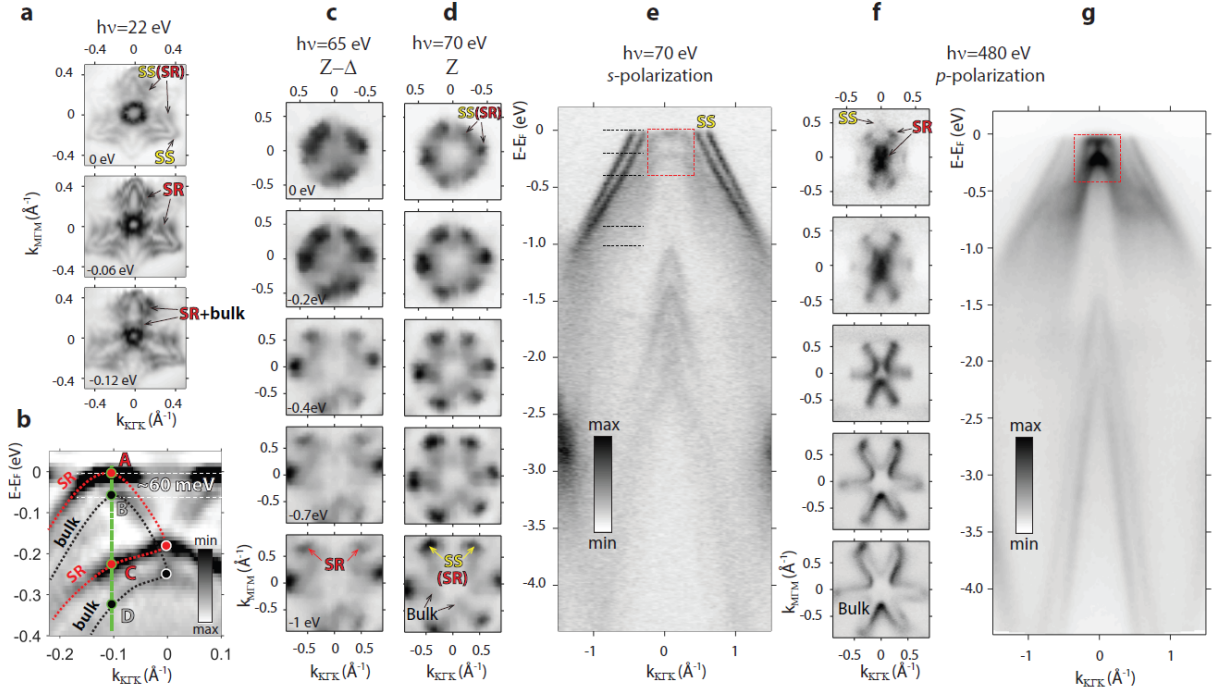


FIG. 2. ARPES band maps and isoenergies near the Z-point of α -GeTe} measured at different photon energies: (a,b) $h\nu=22$ eV; (c-e) 65 and 70 eV; (f,g) 480 eV. ARPES data in (c-e) were measured with *s*-type light polarization, remaining data with *p*-type polarization. The isoenergy surfaces (isoenergies) in panels (c,d,f) were measured at binding energies indicated in panel (e) by horizontal dashed lines. The arrows indicate momenta for pure surface states (SS) and surface resonances (SR) with respect to bulk bands, also indicated in red dashed rectangles in (e) and (g). Panel (b) is a second derivative band map with bulk bands screened by their resonance replica, vertical green line indicate an EDC-cut intersecting the bands in points A-B-C-D.

the free carriers in the system[15]. Figure 1 summarizes the $\text{Ge}_{1-x}\text{Mn}_x\text{Te}$ thin film basic properties in terms of atomic arrangement (panel a), ferromagnetic hysteresis (panel b), surface topography (panel c) and ferroelectric response measured in piezo-force microscopy (panel d). Due to high Mn solubility and high hole concentration, the FM Curie temperatures of $T_C=190$ K is amongst the highest of all FM semiconductors. This new class of materials, termed multiferroic Rashba semiconductors (MUFERS), also display a new type of magneto-electric switching due to entangled Rashba-Zeeman splitting [10].

Nonetheless, this overwhelming panel of physical properties might also hide unconventional pairings because the system naturally possesses bulk type-II superconductivity in a non-centrosymmetric lattice arrangement [16, 17]. For this reason further experimental effort is made to engineer topologically non-trivial systems based on $\text{Ge}_{1-x}\text{Mn}_x\text{Te}$ by adequate doping in order to optimize material conditions for hosting 'Majorana'-like quasiparticles [18].

In this paper, we present a review of the α -GeTe and $\text{Ge}_{1-x}\text{Mn}_x\text{Te}$ surface electronic structure studied by (spin- and) angle-resolved photoemission ((S)ARPES). The first issue we address is to show that α -GeTe is a narrow gap semiconductor in which the bulk bands, buried inside the α -GeTe surface electronic structure probed by ARPES, do not reach the Fermi level in contrast to what was recently claimed [9].

Because there is a conspicuous difference in the ARPES interpretation in this respect, we here demonstrate that pure surface and bulk states can be clearly distinguished in ARPES and that the surface and bulk Dirac points are well separated in energy. Since surface effects are quenched on capped α -GeTe surfaces [4], a direct inspection of bulk states is possible, proving that α -GeTe is a ferroelectric Rashba semiconductor with a band gap of about 60 meV. On the other hand, for uncapped surfaces the bulk band edges are difficult to observe due to the presence of strong surface resonance states. This is especially the case near the Z-point where the band gap is smallest and the Rashba splitting is most pronounced [3, 4]. Adding Mn induces ferromagnetism in α -GeTe rendering $\text{Ge}_{1-x}\text{Mn}_x\text{Te}$ multiferroic at sufficiently low temperature with the magnetization perpendicular to the surface. This ferromagnetism opens a Zeeman gap in the Rashba bands. As shown by SARPES, this moreover leads to a vertical spin polarization at the Z-point of the Brillouin zone that can be switched by reversal of the magnetization. Magneto-electric coupling further enhances the functionality of which the prospects are discussed.

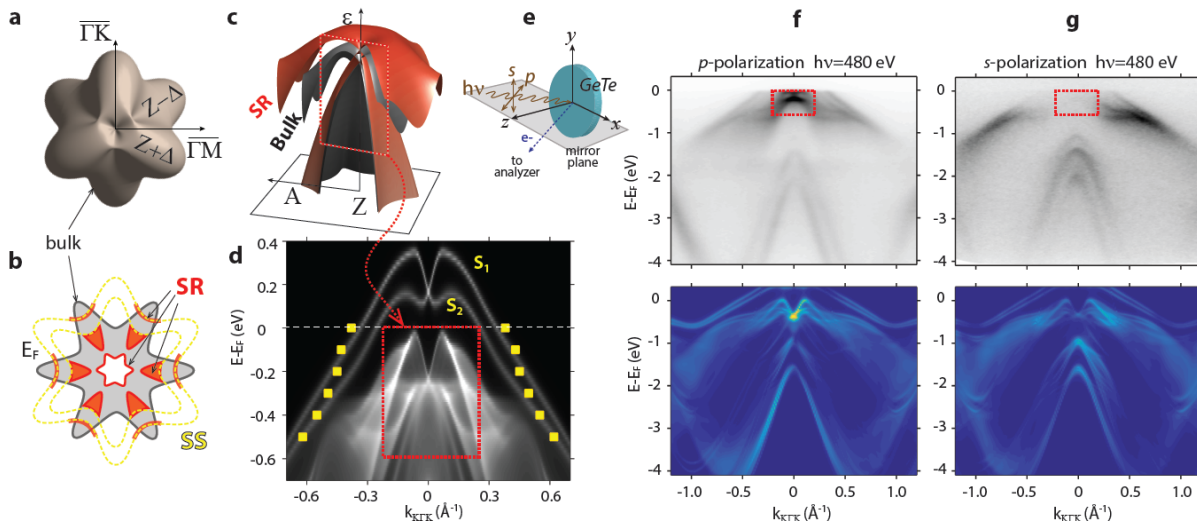


FIG. 3. (a) 3D schematic representation of the α -GeTe bulk isoenergy surface at the Z-point and its vicinity ($Z \pm \Delta$). (b) Schematic projection of the α -GeTe electronic structure onto the surface Brillouin zone; (c) corresponding model of the bulk (black) and bulk-derived SR band (red). (d) α -GeTe semi-infinite crystal calculations, yellow markers indicate the experimentally retrieved dispersion of the surface states $S_{1,2}$ from Fig. 2d. (e) Experimental geometry with p -polarized light. (f, g) ARPES band maps along $\overline{K}\overline{\Gamma}\overline{K}$ measured with p and s -polarized light, respectively. Red frame indicate the energy and momenta with bulk properties, bottom panels are calculations.

α -GeTe SURFACE ELECTRONIC STRUCTURE

To distinguish the surface electronic structure of α -GeTe we compare in Figure 2 ARPES data measured near Z-points with different photon energies of $h\nu$ of 22, 70 and 480 eV at the COPHEE, Pearl and ADDRESS photoemission experimental stations at the Swiss Light Source, respectively. All data were measured at or below 35 K. For each photon energy, constant energy cuts at a given binding energy (isosurfaces) are compared. The isosurfaces at the Z-point in panels a, d and e of Figure 2 have six-fold symmetry, whereas away from the Z-points the isosurfaces assume a three-fold symmetry as seen in panel (c). The schematic picture in Fig. 3(a) illustrates how the 6-fold symmetry at the Z-point changes to three-fold above ($Z + \Delta$) and below ($Z - \Delta$) the Z-point, by showing the top-view of the 3D spindle-torus constant energy surface of α -GeTe[4].

The ARPES data in Fig. 2 shows the influence of the photoelectron escape depth when probing the same electronic structure in surface sensitive vacuum ultraviolet ($h\nu=22$ eV), bulk sensitive soft-X ray ($h\nu=480$ eV) and in-between ($h\nu=70$ eV) [19]. This comparison allows us to identify the surface states (SS), bulk states and the elusive surface resonances (SR). As extensively discussed in Ref.[4], disentangling the SR and bulk bands for α -GeTe near the Z-point is challenging because in the vicinity of the Z-point the SR bands display much higher spectral weight compared to bulk states. Moreover, they disperse with photon energy and are thus easily confused with bulk states [9]. Therefore in ARPES one observes metallic states at E_F , in general agreement with the intrinsic p -type doping from Ge vacancies responsible for the metallic character of the nominally semiconducting GeTe [20]. How-

ever, tunnelling experiments provide firm experimental evidence that α -GeTe is a narrow-gap semiconductor [7]. This gap of around 60 meV can also be seen in Fig. F1(b) buried in the surface electronic structure.

Generally speaking, in photoemission experiments the observation of SR bands is expected to occur around the edge of the projected bulk band structure of semiconductors [21–23]. In this sense, α -GeTe is a textbook example and ignoring the relevance of the SR bands can lead to an erroneous interpretation of the surface electronic structure. This underlines again the importance to combine bulk and surface sensitive photoemission. The data in Fig. 2 reveals the SR-bands detaching from pure surface states in panel (a), progressively enhancing their spectral weight for lower binding energies by forming a 30° rotated isosurface compared to pure surface states. Their density of states near the next Z-point at $h\nu=70$ eV pile-up at the extremities of the hexagonally-warped bulk states (panels c-d), and for the Z-point probed with $h\nu=470$ eV in panel (f) their spectral weight vanishes because of the increased bulk sensitivity.

Projecting all the isosurfaces on the surface plane from surface- and bulk-sensitive ARPES we see a direct deployment of SR bands detaching from the pure surface states and hybridizing with the bulk continuum, as schematically depicted in Fig. 3b in red. Their isosurface projections at selected binding energies shown in Fig. 2d are overlaid with first-principles calculations (yellow markers in Fig. 2d) to show that along the mirror planes (in this case along $\overline{K}\overline{\Gamma}\overline{K}$), the surface resonances follow the dispersion of the two major surface states denoted S_1 and S_2 . We readily see that these surface states have their Dirac point in the unoccupied states because they do not fold back below E_F , and are well sepa-

rated from the bulk states. In Fig. 2c we observe that SR bands outside the Z-point disperse along the bulk bands by changing the isosurfaces from six to three-fold symmetry, which illustrates how the SR bands mimic the bulk bands, and at the same time, in mirror planes they mimic the surface states. Such observation is typical to surface resonances which materialize in the sample sub-surface region comparable with photoelectron escape depth (5-10Å).

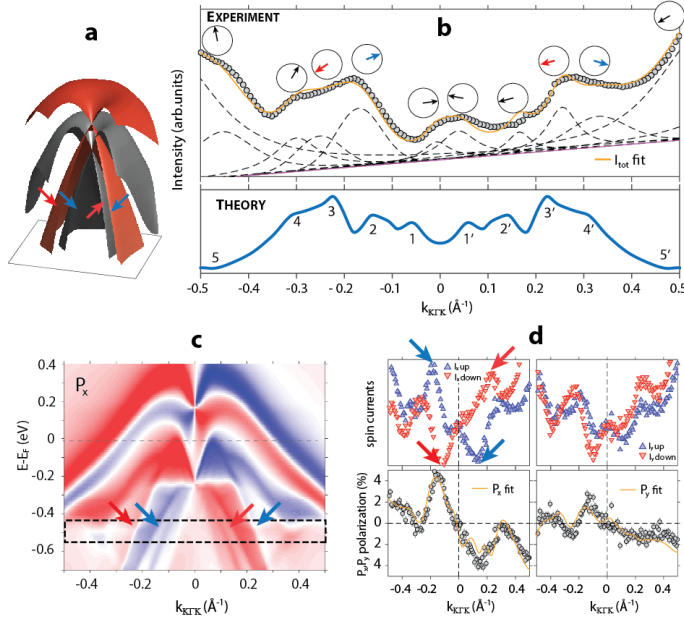


FIG. 4. (a) Simplified surface electronic structure model of the α -GeTe bulk band structure. (b) 3D vectorial spin analysis of data measured along $\overline{\text{KTK}}$ at 0.5 eV binding energy. Theoretical momentum distribution curve (blue line) shows peaks 1-5 and 1'-5', all accounted for in the top panel to fit the total intensity (orange line). The arrows above each peak show the in-plane projection of the spin vector. (c) P_x -spin component of the semi-infinite band-structure calculations in 3d. (d) (bottom) Measured P_x and P_y spin polarization and fits (orange line), and (top) derived spin currents along the resolution-broadened energy range indicated by the dashed rectangle in (c). The main Rashba-type bulk spin splitting is indicated with red/blue arrows in (c) and (d).

Another approach to reveal the dispersive character of the SR-bands in α -GeTe is a k_z -dispersion movie in the $\overline{\text{KTK}}$ mirror plane (see ancillary files). The scan stretches over two Z-points in the 3D Brillouin zone and it shows that upon band-gap opening the SR-band separates from the bulk Rashba band and near the maximum gap at the Γ point ($\hbar\nu \approx 400$ eV) it disappears. As the gap is narrowing again in the k_z -scan, they reappear and disperse side-by-side with the bulk bands toward E_F such that at the Z-point they can be resolved only in a second derivative of the measured band map (Fig. 2b).

From a technological point of view the pure surface Rashba bands $S_{1,2}$ and their resonances are less important because, as already mentioned, on capped α -GeTe surfaces they are completely quenched. Interestingly, their spectral signatures are also easily explored by variation of dipole transition matrix

elements. As shown by Fig. 3f,g, the p and s -polarized light in an experimental geometry depicted in Fig. 3e almost toggles on and off the bulk and bulk-derived bands. This suggests that the dipole selection rules can be used to select the states originating in Ge and Te p_z -orbitals, oriented perpendicular to sample surface along the $\langle 111 \rangle$ direction. This is also confirmed by one-step photoemission calculations on the bottom panels of Fig. 3(f,g), made by a fully relativistic one-step model in its spin-density matrix formulation as implemented in the SPR-KKR package [24, 25].

For a practical description of the α -GeTe bulk electronic structure in surface-sensitive ARPES, Fig. 3(b,c) shows a simple cartoon view of the bulk and bulk-derived SR bands depicted in black and red, respectively. Until new detection schemes in SARPES become available in soft-X regime capable to investigate pure bulk states [19, 26], α -GeTe SARPES data will always integrate the spectral intensity from both the SR and bulk bands, as seen in Fig. 2b. The band map clearly resolves the narrow-gapped bulk states (black dashed lines) and their surface resonance-replica (red dashed lines) screening the bulk states and shifted up to E_F . Visualizing SARPES data with energy distribution curve (EDC) as seen in Fig. 2b one should always keep in mind that the SR and bulk bands intersect these bands in four points denoted A-C for surface-resonances, and B-D for the bulk bands.

EXPERIMENTS VERSUS FIRST-PRINCIPLES CALCULATIONS

To illustrate the validity of the electronic structure model, we compare rigorous first principles calculations to the experimental data. Figure 4 summarizes SARPES data measured in the $\overline{\text{KTK}}$ mirror plane around a binding energy of 0.5 eV along the momenta denoted in the dashed frame in panel (b). The calculations predict that the electronic structure is highly modulated with up to ten peaks labelled 1-5 and 1'-5', respectively. Also the measured spin texture is highly modulated, in our case the appearance of individual peaks is well accounted in both experiment and theory (top panel in Fig. 4b). The

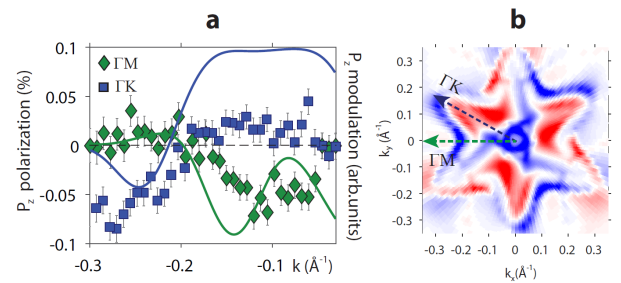


FIG. 5. (a) Out-of-plane spin-polarization P_z measured of α -GeTe at 0.5 eV binding energy along ΓM and $\overline{\Gamma\text{K}}$ (symbols). Full lines show the corresponding P_z modulations for the semi-infinite crystal calculations in (b).

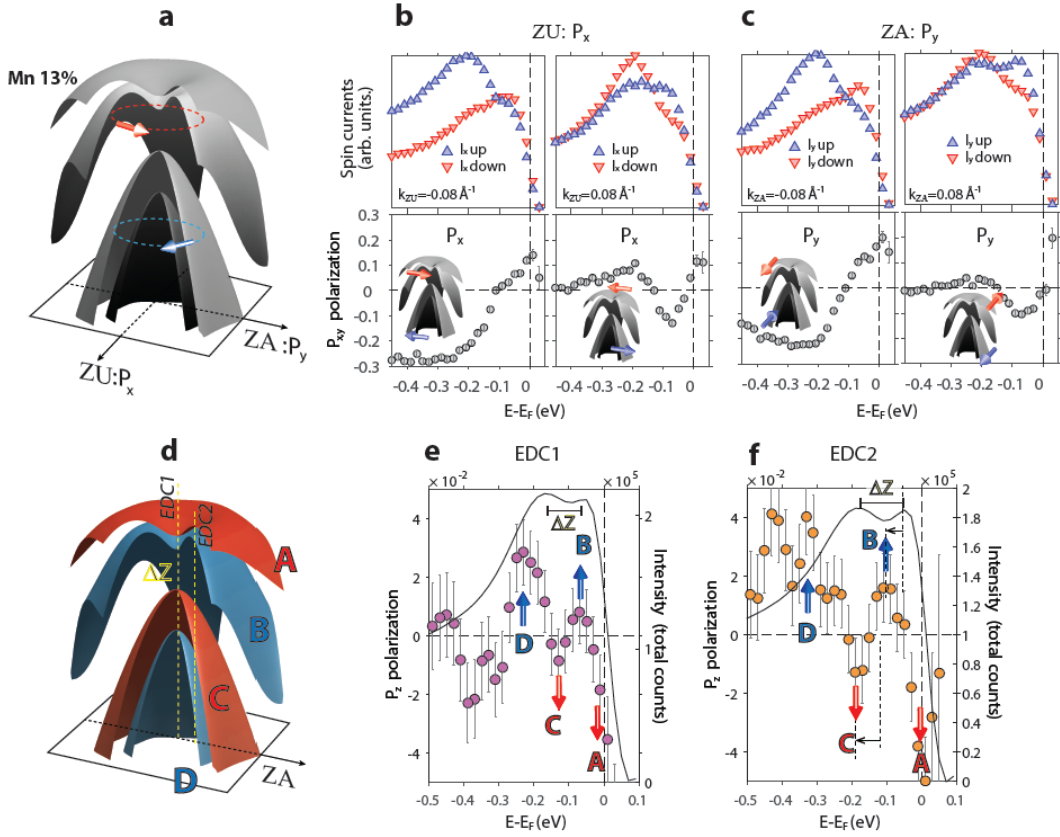


FIG. 6. (a) Simplified surface electronic structure model of the $\text{Ge}_{1-x}\text{Mn}_x\text{Te}$ bulk band structure with in-plane spin texture above and below the Zeeman gap Δ_Z . (b,c) Measured $P_{x,y}$ spin polarization (bottom) and corresponding spin currents (top) for off-normal emission ($\pm 0.08 \text{ \AA}^{-1}$) along Z-U and Z-A directions from $\text{Ge}_{0.87}\text{Mn}_{0.13}\text{Te}$. (d) Simplified model of the out-of-plane spin texture P_z from as-grown $\text{Ge}_{0.87}\text{Mn}_{0.13}\text{Te}$ samples, deduced from data measured in normal (e) and off-normal (f) emission. The red/blue arrows indicate the spin texture, the horizontal arrow in (f) indicate the shift of the bands B-C which define the Zeeman gap of ≈ 100 meV, as observed in the total counts (solid line in e,f).

spin fitting is comprehensively described using a 3D vectorial analysis which fits MDC total intensity and measured 3D spin polarizations [4, 10, 12, 27] (orange lines in Fig. 4b,d). The obtained spin vectors from individual peaks, projected in the $\{x,y\}$ plane (see experimental geometry in Fig. 3e) are shown in Fig. 4a. Consistent with the calculated spin-resolved band-map in panel (c), the main in-plane spin currents are detected along the x -direction. Along that direction there are two prominent spin currents highlighted by the red and blue arrows in panel (d). SARPES MDC maps these currents as two main bulk-like Rashba bands, which is evidenced by their antiparallel $P_{x,y}$ spin vector alignment (red-blue arrows in panel b). We note that the spin-switching of these two bands was extensively tested in *operando* SARPES in field effect devices to show that their manipulation by E-fields is possible [12]. These experimental observations give us confidence that the highly modulated spin texture can indeed be simplified as depicted in panel (a).

Equally highly modulated is the out-of-plane spin-polarization P_z measured at the same binding energy, shown in Fig. 4. SARPES data in panel (a) is visualized as spin-resolved MDCs, which we relate to calculations in panel (b),

measured along the $\overline{\Gamma\text{M}}$ and $\overline{\Gamma\text{K}}$ directions as denoted by blue/green arrows. The measured P_z modulation shows excellent agreement with the first-principles calculations and confirms our detailed understanding of the α -GeTe P_z warping around the Z-point, in agreement with our previous studies [4].

MODIFICATION OF α -GeTe BY MN-DOPING

Figure 6 visualizes SARPES data from $\text{Ge}_{0.87}\text{Mn}_{0.13}\text{Te}$. Panels (a-c) summarize the in-plane $P_{x,y}$ spin windings above and below the Zeeman gap, and panels (d-f) summarize the out-of-plane P_z spin texture. For clarity the simplified surface electronic structure with the Rashba splitting and Zeeman gap is depicted in panel (a). The Zeeman gap opens up around a binding energy of 0.1 eV. In agreement with previous studies [10], the gap size measured in total intensity is $\Delta_Z \approx 100$ meV (Fig. 6e-f). The splitting of the surface electronic structure to B-D bulk and A-C bulk-derived bands becomes evident in the P_z spin texture. In order to confirm the presence of the A-D bands already mentioned in Fig. 2b, data are measured

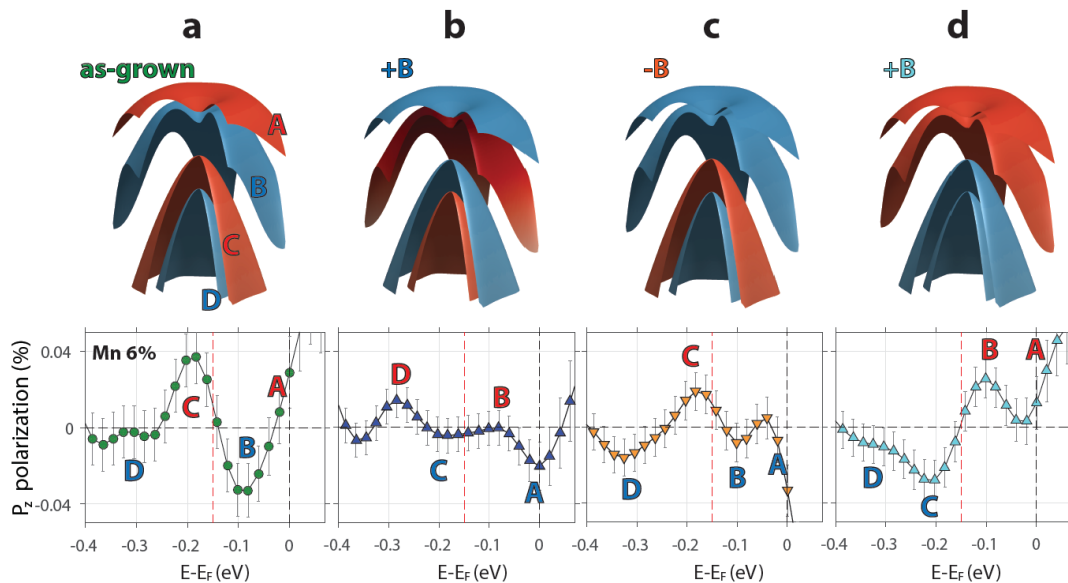


FIG. 7. (a-d) Deployment of the P_z spin-texture of the bands A-D from $\text{Ge}_{0.94}\text{Mn}_{0.06}\text{Te}$ measured in remanent magnetization after magnetizing the sample with ± 700 Gauss (see text for details).

in normal emission (Fig.6e) and off-normal emission (Fig.6f), respectively. The subtle shift in binding energy of the peaks B and C in panel (e) indicated by horizontal arrows in panel (f) is confirming dispersion of all the bands A-D and thus also the simplified electronic scheme of the bulk-derived bands in panels a,d.

FIELD CONTROL OF SPIN TEXTURE

In α -GeTe electric-field control of the spin windings is possible by deposition of a metallic gate electrode on the surface. Applying a gate voltage induces a change in the spin polarization, however, we find that the endurance of the spin switching caused by changing the field direction is limited due to unipolar FE fatigue and other effects such as FE domain pinning [12]. Moreover, epitaxial α -GeTe films typically display a multidomain structure [4, 15, 28] in which polarization reversal may involve intermediate steps via oblique domains rather than direct switching along the $\langle 111 \rangle$ axis which is coupled to the a full spin texture reversal [12].

$\text{Ge}_{1-x}\text{Mn}_x\text{Te}$ appears to have a weaker pinning of the FE polarization because the off-center displacement of the Te atom with respect to the Ge atoms in $\text{Ge}_{1-x}\text{Mn}_x\text{Te}$ decreases with increasing Mn content [15, 29]. This reduces the energy barriers for switching of the atomic positions in the FE reorientation and thus leads to a softening of the FE properties while simultaneously acquiring magnetoelectric properties. Thus, from an application point of view, $\text{Ge}_{1-x}\text{Mn}_x\text{Te}$ fulfills all criteria for mutual control of magnetism and ferroelectricity via magnetoelectric coupling effects, which is a unique material property [30, 31].

In order to emphasize the close relation between α -GeTe and $\text{Ge}_{1-x}\text{Mn}_x\text{Te}$, Fig. 7 summarizes the B-field control of $\text{Ge}_{0.94}\text{Mn}_{0.06}\text{Te}$ in which the size of the Zeeman gap is less than 50 meV [10]. Data were measured at the CASSIOPEE beamline at the Soleil synchrotron in remanent magnetization and show how the P_z spin-texture from as-grown samples develops in consecutive sample magnetization cycles. Contrary to the E-field manipulation of the α -GeTe spin texture in which the spin control is basically stalled after the second cycling, the B-field control from $\text{Ge}_{0.94}\text{Mn}_{0.06}\text{Te}$ is found to change after each sample magnetization. We note that after the third magnetization cycle (Fig. 7d) the P_z spin texture stabilizes in a configuration as predicted by theory for bulk $\text{Ge}_{1-x}\text{Mn}_x\text{Te}$ [10, 12].

SARPES data in Fig. 6-7 confirm that apart from the Zeeman gap, the simplified surface electronic structure model of α -GeTe also applies for $\text{Ge}_{1-x}\text{Mn}_x\text{Te}$ and that manipulating the spin-texture by external fields in photoemission impart additional degrees of freedom associated with surface resonances, as seen in the gradual deployment of the P_z spin-texture in Fig. 7. Our experimental observations suggest that there are certain volatile degrees of freedom in the surface electronic structure and in the spin-texture which give rise to complex switching paths. Consequently they may result in unconventional spin texture evolutions upon manipulation by external fields [10, 12] or by tuning the α -GeTe surface termination. For example the energetically less favorable α -GeTe surface termination with Ge-atoms discussed in Ref. [13] according to the simplified surface electronic structure affects only the top-most surface-resonance sheet A sitting right at E_F , rather than a the full switching which extends to the bulk Rashba bands.

CONCLUSIONS

By comprehensive (S)ARPES mapping of the electronic structure we have evaluated in detail the spin-resolved electronic structure of the ferroelectric and multiferroic Rashba semiconductors α -GeTe and $\text{Ge}_{1-x}\text{Mn}_x\text{Te}$. The strong spin-orbit effect entails large spin splitting of the surface electronic structure consisting of surface and surface resonant states, which are screening the bulk Rashba bands. The different contributions can be separated and analyzed by combining measurements at different photon energies and photon polarizations. Independently of the substrates (BaF_2 , InP or Si [111]) used for thin film deposition, ARPES consistently indicates that all the band types possess their own Dirac point and that the surface states have the Dirac point in the unoccupied states. Our experimental findings are in excellent agreement with *ab-initio* calculations based on the multiple scattering approach, density functional theory and semi-infinite crystal calculations with included spin-orbit coupling, as described in Ref. [4, 10]. This leads to a simplified model of the α -GeTe and $\text{Ge}_{1-x}\text{Mn}_x\text{Te}$ surface electronic structure, its validity is shown by comparison to rigorous *ab-initio* calculations. Our experimental results confirm the coupling between the ferromagnetic and ferroelectric order in $\text{Ge}_{1-x}\text{Mn}_x\text{Te}$ because the Rashba-type spin texture is clearly influenced by the magnetization switching. This is the main precondition for functional spintronic applications, but presently the magneto-electric coupling imposes limited functionality due to the complex switching paths of the Rashba spin textures even at temperatures around 35 K.

ACKNOWLEDGEMENTS

This work was supported by the Swiss National Science Foundation Project No. PPO0P2_1447421 and n.200021 146890. G.S. and V.V.V. acknowledge support from the Austrian Science Funds (SFB-025, IRON). JM would like to thank CEDAMNF project (CZ.02.1.01/0.0/0.0/15_003/0000358) funded by the Ministry of Education, Youth and Sports of Czech Republic.

-
- [1] J. Nitta, T. Akazaki, H. Takayanagi, and T. Enoki, *Phys. Rev. Lett.* **78**, 1335 (1997).
- [2] M. Maekawa, ed., *Concepts in Spin Electronics* (Oxford University Press, 2006) pp. 43–90.
- [3] D. Di Sante, P. Barone, R. Bertacco, and S. Picozzi, *Advanced Materials* **25**, 509 (2013).
- [4] J. Krempaský, H. Volfová, S. Muff, N. Pilet, G. Landolt, M. Radović, M. Shi, D. Kriegner, V. Holý, J. Braun, H. Ebert, F. Bisti, V. A. Rogalev, V. N. Strocov, G. Springholz, J. Minár, and J. H. Dil, *Phys. Rev. B* **94**, 205111 (2016).
- [5] P. Fons, A. V. Kolobov, M. Krbal, J. Tominaga, K. S. Andrikopoulos, S. N. Yannopoulos, G. A. Voyiatzis, and T. Uruga, *Phys. Rev. B* **82**, 155209 (2010).
- [6] M. Wuttig, D. Lusebrink, D. Wamwangi, W. Welnic, M. Gilleszen, and R. Dronskowski, *Nat. Mater.* **6**, 122 (2007).
- [7] L. Esaki, in *Proc. Intern. Conf. Semicond. Phys.* (1966) p. 589.
- [8] G. S. Pawley, W. Cochran, R. A. Cowley, and G. Dolling, *Phys. Rev. Lett.* **17**, 753 (1966).
- [9] M. Liebmann, C. Rinaldi, D. Di Sante, J. Kellner, C. Pauly, R. N. Wang, J. E. Boschker, A. Giussani, S. Bertoli, M. Cantoni, L. Baldrati, M. Asa, I. Vobornik, G. Panaccione, D. Marchenko, J. Sanchez-Barriga, O. Rader, R. Calarco, S. Picozzi, R. Bertacco, and M. Morgenstern, *Advanced Materials* **28**, 560 (2016).
- [10] J. Krempaský, S. Muff, F. Bisti, M. Fanciulli, H. Volfová, A. P. Weber, N. Pilet, P. Warnicke, F. Bertran, H. Ebert, J. Braun, J. Minár, G. Springholz, J. Dil, and V. Strocov, *Nat. Commun.* **7**, 13071 (2016).
- [11] H. J. Elmers, R. Wallauer, M. Liebmann, J. Kellner, M. Morgenstern, R. N. Wang, J. E. Boschker, R. Calarco, J. Sánchez-Barriga, O. Rader, D. Kutnyakhov, S. V. Chernov, K. Medjanik, C. Tusche, M. Ellguth, H. Volfova, S. Borek, J. Braun, J. Minár, H. Ebert, and G. Schönhense, *Phys. Rev. B* **94**, 201403 (2016).
- [12] J. Krempaský, S. Muff, J. Minár, N. Pilet, M. Fanciulli, A. Weber, V. Volobuev, M. Gmitra, C. Vaz, V. Scagnoli, G. Springholz, and J. Dil, arXiv:1707.08431v1 [cond-mat.mtrl-sci] (2017).
- [13] C. C. Rinaldi, S. Varotto, M. Asa, J. Slawinska, J. Fujii, G. Vinai, S. Cecchi, R. Calarco, I. Vobornik, G. Panaccione, S. Picozzi, and B. R., arXiv:1707.07043v1 [cond-mat.mtrl-sci] (2017).
- [14] S. Picozzi, *Frontiers in Physics* **2** (2014).
- [15] H. Przybylińska, G. Springholz, R. T. Lechner, M. Hassan, M. Wegscheider, W. Jantsch, and G. Bauer, *Phys. Rev. Lett.* **112**, 047202 (2014).
- [16] P. Stiles, L. Esaki, and J. Schooley, *Physics Letters* **23**, 206 (1966).
- [17] V. Narayan, T.-A. Nguyen, R. Mansell, D. Ritchie, and G. Musler, *physica status solidi (RRL) Rapid Research Letters* **10**, 253 (2016).
- [18] C. W. J. Beenakker, *Annual Review of Condensed Matter Physics* **4**, 113 (2013).
- [19] C. S. Fadley, *Synchrotron Radiation News* **25**, 26 (2012).
- [20] A. H. Edwards, A. C. Pineda, P. A. Schultz, M. G. Martin, A. P. Thompson, H. P. Hjalmarson, and C. J. Umrigar, *Phys. Rev. B* **73**, 045210 (2006).
- [21] M.-C. Desjonquères and D. Spanjaard, *Concepts in Surface Physics* (Springer, 1998).
- [22] P. Yu and M. Cardona, *Fundamentals of semiconductors, Physics and Materials Properties* (Springer-Verlag Berlin Heidelberg, 2010) pp. 430–490.
- [23] L. Ley and M. Cardona, eds., *Photoemission in Solids II* (Springer-Verlag Berlin Heidelberg, 1979) pp. 63–67.
- [24] H. Ebert, D. Ködderitzsch, and J. Minár, *Rep. Prog. Phys.* **74** (2011).
- [25] J. Braun, K. Miyamoto, A. Kimura, T. Okuda, M. Donath, H. Ebert, and J. Minár, *New Journal of Physics* **16**, 015005 (2014).
- [26] V. N. Strocov, V. N. Petrov, and J. H. Dil, *Journal of Synchrotron Radiation* **22**, 708 (2015).
- [27] F. Meier, J. H. Dil, and J. Osterwalder, *New J. Phys.* **11**, 125008 (2009).
- [28] R. Wang, J. E. Boschker, E. Bruyer, D. D. Sante, S. Picozzi, K. Perumal, A. Giussani, H. Riechert, and R. Calarco, *The Journal of Physical Chemistry C* **118**, 29724 (2014).

- [29] D. Kriegner, J. Furthmüller, R. Kirchschrager, J. Endres, L. Horak, P. Cejpek, H. Reichlova, X. Marti, D. Primetzhofer, A. Ney, G. Bauer, F. Bechstedt, V. Holy, and G. Springholz, *Phys. Rev. B* **94**, 054112 (2016).
- [30] W. Eerenstein, N. D. Mathur, and J. F. Scott, *Nature* **442**, 759 (2006).
- [31] M. Fiebig, *Journal of Physics D: Applied Physics* **38**, R123 (2005).